Measurement and Modeling of Ca^{2+} Waves in Isolated Rabbit Ventricular Cardiomyocytes

N. MacQuaide,* J. Dempster,† and G. L. Smith*
*Institute of Biomedical and Life Sciences, University of Glasgow, Glasgow, United Kingdom; and †Department of Physiology and Pharmacology, University of Strathclyde, Glasgow, United Kingdom

ABSTRACT The time course and magnitude of the Ca^{2+} fluxes underlying spontaneous Ca^{2+} waves in single permeabilized ventricular cardiomyocytes were derived from confocal Fluo-5F fluorescence signals. Peak flux rates via the sarcoplasmic reticulum (SR) release channel (RyR2) and the SR Ca^{2+} ATPase (SERCA) were not constant across a range of cellular [Ca^{2+}] values. The Ca^{2+} affinity (K_{mf}) and maximum turnover rate (V_{max}) of SERCA and the peak permeability of the RyR2-mediated Ca^{2+} release pathway increased at higher cellular [Ca^{2+}] loads. This information was used to create a computational model of the Ca^{2+} wave, which predicted the time course and frequency dependence of Ca^{2+} waves over a range of cellular Ca^{2+} loads. Incubation of cardiomyocytes with the Ca^{2+} calmodulin (CaM) kinase inhibitor autocamtide-2-related inhibitory peptide (300 nM, 30 mins) significantly reduced the frequency of the Ca^{2+} waves at high Ca^{2+} loads. Analysis of the Ca^{2+} fluxes suggests that inhibition of CaM kinase prevented the increases in SERCA V_{max} and peak RyR2 release flux observed at high cellular [Ca^{2+}]. These data support the view that modification of activity of SERCA and RyR2 via a CaM kinase sensitive process occurs at higher cellular Ca^{2+} loads to increase the maximum frequency of spontaneous Ca^{2+} waves.

INTRODUCTION

In the heart, ventricular cardiomyocytes contain regular arrays of clusters of type 2 ryanodine receptors (RyR2), i.e., sarcoplasmic reticulum (SR) Ca^{2+} channels. These channels can open spontaneously and generate a limited nonpropagating Ca^{2+} release event termed a Ca^{2+} spark (1). Under certain circumstances, a Ca^{2+} spark can trigger Ca^{2+} release from adjacent RyR2 clusters in a regenerative manner, propagating throughout a ventricular myocyte in the form of a Ca^{2+} wave (2–5). Spontaneous Ca^{2+} waves during diastole are indicative of cellular Ca^{2+} overload; the beneficial consequences are thought to be twofold: i), to minimize the diastolic tone associated with a certain degree of Ca^{2+} overload (6); and ii), to stimulate Ca^{2+} extrusion from the cell (7). However, the spontaneous Ca^{2+} release generates an after depolarization that can be arrhythmogenic (2,8). In an effort to understand the cellular mechanisms responsible for spontaneous Ca^{2+} release, this phenomenon has been studied under a range of experimental conditions in intact (7,9) and permeabilized cardiac cells (10,11). Increased intracellular [Ca^{2+}] increases the frequency but not the amplitude of spontaneous Ca^{2+} release, suggesting a fixed intra-SR threshold [Ca^{2+}] for release (2,7,11). But this mechanism may not apply at very high intracellular Ca^{2+} values (11,12). Additional insight into the subcellular events underlying Ca^{2+} waves has come from computational modeling studies. This work has examined the conditions necessary for Ca^{2+} wave propagation (13–15), but have not attempted to predict Ca^{2+} wave time course or frequency at different intracellular [Ca^{2+}] levels. This study examines the characteristics of the Ca^{2+} waves in permeabilized ventricular myocytes at a range of intracellular Ca^{2+} loads. Computational modeling suggests that mean cytoplasmic [Ca^{2+}] modulates the peak rates of SR Ca^{2+} release and uptake. Inhibition of Ca^{2+} calmodulin (CaM) kinase removed the Ca^{2+} sensitivity of these fluxes suggesting a causal link.

MATERIALS AND METHODS

Cell isolation and permeabilization

Ventricular myocytes were isolated from Langendorff perfused rabbit hearts by enzymatic digestion as previously described (16). Isolated cells were maintained in a modified Krebs solution buffered with 1 mM ethylene bis[oxyethylenenitrilo] tetraacetic acid (EGTA) at a concentration of $\sim 10^4$ cells/ml until use. The cells were allowed to settle onto the coverslip at the base of a small bath. β-escin (Sigma, St. Louis, MO) was added from a freshly prepared stock solution to the cell suspension to give a final concentration of 0.1 mg/ml for 0.5–1 min and the β-escin subsequently removed by perfusion with a mock intracellular solution (see below).

Solutions

Permeabilized cells were perfused with a mock intracellular solution with the following composition (mM): 100 KCl, 5 K_2ATP, 5Na_2CrP, 5.5 $MgCl_2$, 25 HEPES, 0.05 K_2EGTA, pH 7.0 (20–21°C). The [Ca^{2+}] in the perfusing solution was varied by the addition of known amounts of 1 M $CaCl_2$ stock solution (BDH, UK). Fluorescent Ca^{2+} indicators Fluo-3 or Fluo-5F (Molecular Probes, Eugene, OR) were added to the solution to give a nominal final concentration of 10 μM. Myocyte contraction was minimized by the inclusion of 10 μM cytochalasin-D; separate measurements confirmed that this concentration of cytochalasin-D does not affect the SR Ca^{2+} release or uptake processes and had no effect on spontaneous Ca^{2+} wave frequency. Autocamtide-2-related inhibitory peptide(AIP) (CalBiochem, San Diego, CA) was used in the myristoylated form at a concentration of 300 nM. Intact

Submitted December 22, 2006, and accepted for publication May 29, 2007.
Address reprint requests to G. L. Smith, Tel.: 44-141-330-5963; Fax: 44-141-330-4612; E-mail: g.smith@bio.gla.ac.uk.
Editor: David A. Eisner.

0006-3495/07/10/2581/15 $2.00
doi: 10.1529/biophysj.106.102293

cells were incubated for 30 mins with AIP before β-escin treatment. All solutions used subsequently contained 300 nM AIP.

Data recording and analysis

Confocal line-scan images were recorded using a BioRad (Cambridge, MA) Radiance 2000 confocal system. The Fluo-5F in the perfusing solution was excited at 488 nm and measured above 515 nm using epifluorescence optics of a Nikon (Tokyo, Japan) Eclipse inverted microscope with a Fluor 60× water objective lens (N.A. 1.2). Iris diameter was set at 1.9 providing an axial (z) resolution of ~0.9 μm and X-Y resolution of ~0.5 μm based on fullwidth half-maximal amplitude measurements of images of 0.1 μm fluorescent beads (Molecular Probes). Data were acquired in line-scan mode at 2 ms/line; pixel dimension was 0.3 μm (512 pixels/scan; zoom = 1.4). The scanning laser line was oriented parallel with the long axis of the cell and placed approximately equidistant between the outer edge of the cell and the nucleus/nuclei, to ensure the nuclear area was not included in the scan line. As illustrated in Fig. 1 *A*, the LaserScan (BioRad) software saved the data as a series of image files each containing 30,000 line scans (i.e., 1 min of continuous recording). An experimental record typically comprised four to five line-scan image files; these were reviewed offline and a single intracellular region (80 pixels wide) was selected close to the origin of the wave (indicated in Fig. 1 *A*). Every protocol was followed by a series of three Ca^{2+} calibration solutions, identical in composition to the experimental solutions apart from containing 10 mM EGTA and a free [Ca^{2+}] of: i), 1 nM; ii), 380 nM; and iii), 60 μM. The subsequent intracellular and extracellular fluorescence signals were used to convert the previous fluorescence signals to intracellular [Ca^{2+}] as described previously (11) and detailed in the online Supplementary Material. Conversion of fluorescence to [Ca^{2+}] was accomplished assuming a Fluo5F K_d of 1.04 μM (17).

Wave detection and velocity correction

Measurements of Ca^{2+} wave velocity along the length of the myocyte were made using a cross-correlation method similar to that described previously (1). Briefly, a line-scan image of Fluo-5F fluorescence was divided into 10 pixel bands. Cross correlation of individual Ca^{2+} wave signals gave a measure of the time taken to propagate eight sequential 3-μm segments along the length of the cardiomyocyte. The mean velocity over an 80 pixel (24 μm) segment was calculated for eight sequential Ca^{2+} waves recorded in the steady state. The cross-correlation technique was also used to align the waveforms of the Ca^{2+} wave recorded in 8 × 10 pixel bands. The series of aligned signals were used to generate an average fluorescence signal of a Ca^{2+} wave in an 80-pixel region of the cardiomyocyte.

Three-compartment model of Ca^{2+} fluxes in a permeabilized cardiomyocyte

Cytoplasmic [Ca^{2+}] in a subcompartment of a cardiac myocyte during a Ca^{2+} wave was reconstructed using a three-compartment model (Supplementary Fig. 1). Estimates of the magnitude and time course of the various Ca^{2+} flux pathways were derived from experimental measurements in permeabilized cardiac myocytes. Cytoplasmic [Ca^{2+}] from a resolution limited volume of a cardiac myocyte during the Ca^{2+} wave was calculated from confocal Fluo-5F fluorescence signals. These values in conjunction with estimates for intracellular buffering and the diffusion rate constant were used to calculate the underlying Ca^{2+} fluxes. This approach was based on the assumption that once initiated, the Ca^{2+} wave in cardiac muscle is a one-dimensional wave; i.e., effectively the Ca^{2+} wave occurred simultaneously throughout the depth and width of the cell. Evidence for assumption comes from experimental measurements that indicated that the Ca^{2+} wave is essentially planar in both z axis (cell depth) and x axis (cell width) (4,15). The consequence of the planar wave is that the gradient of cytoplasmic

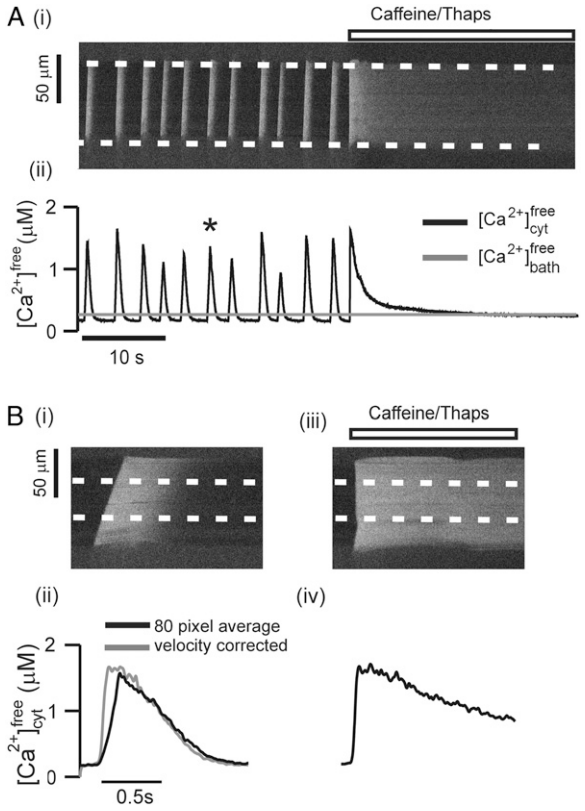

FIGURE 1 (*A* (*i*)) A typical line-scan epifluorescence image of a single permeabilized cardiomyocyte perfused with 280 nM Ca^{2+} (in 50 μM EGTA, 10 μM Fluo-3). The brighter central region is due to Fluo-5 in the cell, dimmer flanking signals are from the Fluo-5 in the perfusing solutions. White dashed lines denote an 80-pixel band within the cytosol. Superfusion with 10 mM caffeine and 25 μM Thapsigargin is indicated above the image. (*A* (*ii*)) Black line, $[Ca^{2+}]^{free}_{cyt}$ signal derived from the mean fluorescence signal of the 80-pixel region within the cell marked in panel above; gray line, $[Ca^{2+}]^{free}_{bath}$ in the perfusing solution calculated from the extracellular Fluo-5 fluorescence signal. (*B* (*i*)) Line-scan epifluorescence image of a single Ca^{2+} wave (marked by * in panel *A* (*i*)). (*B* (*ii*)) Black line, $[Ca^{2+}]^{free}_{cyt}$ signal derived from the mean fluorescence signal of the 80-pixel region within the cell; gray line, the average $[Ca^{2+}]^{free}_{cyt}$ after correction for the velocity of wave propagation. (*B* (*iii* and *iv*)) Line-scan image of the rapid application of caffeine and the corresponding $[Ca^{2+}]^{free}_{cyt}$ values calculated from the marked 80-pixel section. Both signals were filtered using adjacent averaging (five-point).

[Ca^{2+}] and therefore diffusion in the z and x axis is small. Behind the wave front (e.g., 2 μm) in the y axis, the cytoplasmic [Ca^{2+}] is still high from the passing Ca^{2+} wave (having occurred ~20 ms earlier). In advance of the wave front in the y axis is the only direction with a significant cytoplasmic [Ca^{2+}] concentration gradient and the potential for diffusion. The sharp wave front observed (within the spatial resolution of the confocal (5)) suggests that over the timescale of the release event (<1 s) diffusion is minimal. The three-compartment model also assumes that diffusion of Ca^{2+} within the SR is minimal. Measured values of the luminal Ca^{2+} diffusion coefficient (50–60 $\mu m s^{-2}$) (18,19) indicate that intra-SR movement of Ca^{2+} during the time course of the wave is small.

The method by which the change in free cytoplasmic Ca^{2+} ($[Ca^{2+}]^{free}_{cyt}$) under a range of conditions was used to calculate the Ca^{2+} fluxes and free intra-SR ($[Ca^{2+}]^{free}_{SR}$) within a resolution-limited volume of permeabilized cardiac myocyte using a three-compartment model is illustrated in Supplementary Fig. 1. Assuming the free [Ca^{2+}] in the bath solution ($[Ca^{2+}]^{free}_{bath}$)

was constant ($dCa_{bath}^{free}/dt = 0$), the differential equations describing the change of free [Ca^{2+}] within the cytoplasm and SR were as follows:

$$\frac{dCa_{cyt}^{free}}{dt} = f_{cyt}^{buffer}(J_{RyR} - J_{SERCA} + J_{Diff}) \quad (1)$$

$$\frac{dCa_{SR}^{free}}{dt} = f_{SR}^{buffer}(J_{SERCA} + J_{RyR}). \quad (2)$$

SERCA-mediated Ca^{2+} flux (J_{SERCA}) was described using a previously published equation (20) (see Appendix, Eq. A1). The Ca^{2+} flux due to diffusion between the cytoplasm and the extracellular space (J_{diff}) was measured experimentally (Appendix, Eq. A2). The periodic changes in RyR2-mediated flux (J_{RyR}) was modeled using the following conditions:

$$\text{If}[Ca^{2+}]_{SR}^{free} < [Ca^{2+}]_{SR}^{threshold} \text{ then : } J_{RyR} = J_{leak}.$$

$$\text{If}[Ca^{2+}]_{SR}^{free} \geq [Ca^{2+}]_{SR}^{threshold} \text{ then : } J_{Ryr} = J(t)_{wave} + J_{leak}.$$

$[Ca]_{SR}^{threshold}$ is the calculated maximum value of $[Ca^{2+}]_{SR}^{free}$ based on experimental measurements of total SR Ca^{2+} content. J_{leak} is the background Ca^{2+} leak from the SR (see Appendix, Eq. A3) and is presumed to be mainly via spontaneous activity of RyR2. The magnitude of this flux pathway was measured experimentally (see Fig. 5). $J(t)_{wave}$ is a time-dependant change in RyR2 permeability; the time course and extent was calculated from measurements made on permeabilized cells. The function f_{cyt}^{buffer} transforms the net Ca^{2+} flux in the cytosol to a change in $[Ca^{2+}]_{cyt}^{free}$. This function used previously published measurements of cytosolic Ca^{2+} binding in permeabilized rabbit cardiac myocytes (21) (see Appendix, Eq. A4).

Equation 2 is used to quantify the change $[Ca^{2+}]_{SR}^{free}$, whereas f_{SR}^{buffer} transforms the net Ca^{2+} flux in the SR a change in $[Ca^{2+}]_{SR}^{free}$ based on previously published estimates of the concentration and binding capacity of Ca^{2+} buffers in rabbit cardiomyocytes (20) (see Appendix, Eq. A5).

RESULTS

Measurement of Ca^{2+} waves in permeabilized single myocytes

Fig. 1 *A* shows a typical line-scan image from a permeabilized rabbit ventricular cardiomyocyte perfused with a solution containing 280 nM Ca^{2+}. This solution caused regular Ca^{2+} waves (~0.2 Hz) that propagated the full length of the cardiomyocyte. At the point indicated, 10 mM caffeine and 25 μM thapsigargin were rapidly applied to release Ca^{2+} from the SR and to inhibit reuptake. The horizontal dashed lines delineates an 80-pixel region (24 μm) along the scan line through the permeabilized myocyte. Fig. 1 *A* (*ii*) shows time course of $[Ca^{2+}]_{cyt}^{free}$ (*black line*) and $[Ca^{2+}]_{bath}^{free}$ (*gray line*) derived from the average fluorescence signal from the 80-pixel band within the cell and a comparable region in the extracellular space adjacent to the cell, respectively. Note that after prolonged perfusion with caffeine/thapsigargin, the $[Ca^{2+}]_{cyt}^{free}$ signal is equal to the $[Ca^{2+}]_{bath}^{free}$, indicating equilibration of the [Ca^{2+}] within the two compartments. The same situation exists before addition of caffeine, despite the oscillating level of $[Ca^{2+}]_{cyt}^{free}$, the mean $[Ca^{2+}]_{cyt}^{free}$ over a period of 2–4 s is equal to the $[Ca^{2+}]_{bath}^{free}$ (11). Fig. 1 *B* (*i*) shows the line-scan image of the Ca^{2+} wave on a faster time base with an 80-pixel central region indicated. The sloping wave front represents the propagation of the Ca^{2+} wave from one end of the cell to the other at an approximately constant velocity (~120 μm/s). The diagram in Fig. 1 *B* (*ii*) shows the time course of the $[Ca^{2+}]_{cyt}^{free}$ in the 80-pixel section (*black line*). The gray line represents the time course after correction of the wave front for the smearing of the upstroke caused by the propagation of the Ca^{2+} wave over the ~24 μm (80 pixels) within the cell (see Methods). Panels *iii* and *iv* are the corresponding line-scan image and $[Ca^{2+}]_{cyt}^{free}$ from the cell during rapid application of caffeine/thapsigargin. On addition of caffeine, the rise of $[Ca^{2+}]_{cyt}^{free}$ is approximately synchronous along the length of the cell, and the upstroke and amplitude of the $[Ca^{2+}]_{cyt}^{free}$ signal is similar to that of the corrected Ca^{2+} wave. The decline of the $[Ca^{2+}]_{cyt}^{free}$ signal in the presence of caffeine/thapsigargin is considerably slower than the Ca^{2+} wave due to the inability of the SR Ca^{2+} pump to sequester the Ca^{2+}; this decline reflects the loss of Ca^{2+} from the cardiomyocyte by diffusion. In these measurements caffeine causes a small (~10%) but significant quench of the Fluo-5F fluorescence. This was evident from the extracellular fluorescence signal. The time course and extent of caffeine-induced quench was quantified and used to correct the intracellular signal. This correction was minimal during the initial rise of $[Ca^{2+}]_{cyt}^{free}$.

Ca^{2+} waves at a range of perfusing [Ca^{2+}] values

Fig. 2 *A* shows records of $[Ca^{2+}]_{cyt}^{free}$ recorded from 80-pixel regions of line scans recorded from cardiomyocytes exposed to solutions containing Fluo-5F and a range of $[Ca^{2+}]_{bath}^{free}$ (~300 nM (*i*), ~600 nM (*ii*), and ~900 nM (*iii*)). The gray line in each panel indicates the $[Ca^{2+}]_{bath}^{free}$ in each experiment. As the $[Ca^{2+}]_{bath}^{free}$ was increased, Ca^{2+} wave frequency, and minimum and maximum $[Ca^{2+}]_{cyt}^{free}$ all increased. Average values of these parameters are shown in Fig. 2 *B* (*i*). The gray line is the unity relationship between mean $[Ca^{2+}]_{cyt}^{free}$ and $[Ca^{2+}]_{bath}^{free}$. The values of mean $[Ca^{2+}]_{cyt}^{free}$ during a 30-s period of Ca^{2+} waves follows the unity relationship indicating that over the range of 300–900 nM there is no net diffusion of Ca^{2+} between the cytosol and the extracellular space despite the oscillation of $[Ca^{2+}]_{cyt}^{free}$. The relationship between the maximum $[Ca^{2+}]_{cyt}^{free}$ and $[Ca^{2+}]_{bath}^{free}$ was nonlinear, the increase observed from ~600 to 900 nM was much greater than that seen between 300 and 600 nM. Fig. 2 *B* (*ii*) shows the mean values of Ca^{2+} wave frequency versus $[Ca^{2+}]_{bath}^{free}$, the relationship with respect to $[Ca^{2+}]_{cyt}^{free}$ was also nonlinear. The increase in frequency observed between 600 and 900 nM was considerably less than that seen from 300 to 600 nM. The average Ca^{2+} wave velocities showed a similar nonlinear relationship to frequency. At a $[Ca^{2+}]_{bath}^{free} \sim 300$ nM, wave velocity was 130 ± 4 μm/s; at ~900 nM the frequency of the Ca^{2+} waves had increased approximately fivefold whereas the velocity had increased to 180 ± 5 μm/s ($P < 0.05$).

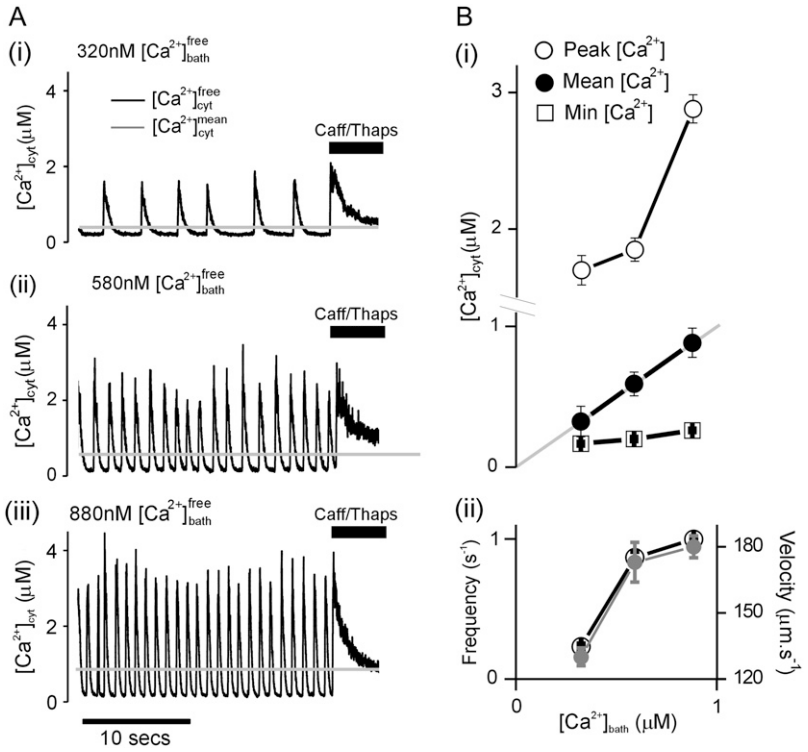

FIGURE 2 (*A*) $[Ca^{2+}]_{cyt}^{free}$ signals derived from the mean Fluo-5 fluorescence signals from: black line, 20-pixel region within cardiomyocytes ($[Ca^{2+}]_{cyt}^{free}$); gray line, the corresponding region in the extracellular space ($[Ca^{2+}]_{bath}^{free}$). At the time indicated the cardiomyocytes were perfused with 10 mM caffeine and 25 μM thapsigargin. (*i*) $[Ca^{2+}]_{bath}^{free}$ = 320nM; (*ii*) $[Ca^{2+}]_{bath}^{free}$ = 580nM; (*iii*) $[Ca^{2+}]_{bath}^{free}$ = 880nM. (*A* (*i*) and *B* (*i*)) Plot of $[Ca^{2+}]_{bath}^{free}$ versus maximum $[Ca^{2+}]_{cyt}^{free}$ (wave peak, ○), mean $[Ca^{2+}]_{cyt}^{free}$ (●), and minimum free $[Ca^{2+}]_{cyt}^{free}$ (□). The gray line indicates the unity relationship. (*ii*) Plot of $[Ca^{2+}]_{bath}^{free}$ versus frequency of Ca^{2+} waves (○) and velocity (●).

Conversion to total cytoplasmic [Ca^{2+}]

Fig. 3 *A* shows the process of conversion of $[Ca^{2+}]_{cyt}^{free}$ signal to total cellular [Ca^{2+}] ($[Ca^{2+}]_{cyt}^{total}$) using the intracellular Ca^{2+}-buffer characteristics measured for digitonin-treated rabbit ventricular myocytes in previous studies (21). The change in $[Ca^{2+}]_{cyt}^{total}$ was derived from eight sequential velocity-corrected Ca^{2+} waves recorded in the steady state (Fig. 2 *A*). As shown in Fig. 3 *A* (*ii*), although the amplitude of the $[Ca^{2+}]_{cyt}^{free}$ signals at 600 nM was larger than that at 300 nM; the amplitude of the two $[Ca^{2+}]_{cyt}^{total}$ signals is similar. This is confirmed by the mean data shown in Fig. 3 *C* (*i*) and suggests that over a range of cellular Ca^{2+} loads, the total [Ca^{2+}] released by the SR during a Ca^{2+} wave is constant irrespective of the mean $[Ca^{2+}]_{cyt}^{free}$ and frequency. Furthermore, the similarity of the amplitude Ca^{2+} wave and caffeine-induced Ca^{2+} release indicates that the Ca^{2+} wave releases the majority of the available SR Ca^{2+} (Fig. 3 *B*). Therefore the increase in the $[Ca^{2+}]_{cyt}^{total}$ of ~150 μM during a Ca^{2+} wave or caffeine transient provides an estimate of the total Ca^{2+} content of the SR under these conditions. Using previously published estimates of SR volume, concentration of intra-SR Ca^{2+} buffer and the apparent K_d of Ca^{2+} (20), these values predict that maximum [Ca^{2+}] in the SR ($[Ca^{2+}]_{SR}^{total}$) is ~3 mM and the free intra-SR Ca^{2+} ($[Ca^{2+}]_{SR}^{free}$) is ~1 mM. The average value of $[Ca^{2+}]_{SR}^{total}$ predicted at a mean $[Ca^{2+}]_{cyt}^{free}$ of ~300 nM was not significantly different from that calculated at 600 and 900 nM and supports the earlier contention that spontaneous SR Ca^{2+} release occurs at a fixed intraluminal [Ca^{2+}] (7,10). An important additional conclusion is that locally, the Ca^{2+} released during a Ca^{2+} wave depletes the SR Ca^{2+} as effectively as caffeine-induced Ca^{2+} release. One source of error in this estimation is the variable timing of the caffeine-induced Ca^{2+} release relative to the preceding Ca^{2+} wave. Releasing Ca^{2+} with caffeine shortly after a Ca^{2+} wave may underestimate the maximum Ca^{2+} content of the SR since refilling may be incomplete. An estimation of the relationship between SR Ca^{2+} content and the time after the preceding wave can be gleaned from a plot between Ca^{2+} wave amplitude and the interwave interval. Fig. 3 *C* shows this relationship based on data from permeabilized cells at ~300, ~600, and 900 nM. This plot shows a shallow dependence of SR Ca^{2+} released during a Ca^{2+} wave and the interwave interval. The data suggest that Ca^{2+} release at periods >60% of the maximum interwave interval will release >90% of the Ca^{2+} released at the longest interwave interval. Therefore if the caffeine-induced Ca^{2+} release is in the latter 50% of the interwave interval it will not substantially underestimate maximum SR Ca^{2+} content. This time course of SR refilling is supported by the predictions from the computational model (see Fig. 8).

Estimation of rate of loss of Ca^{2+} from the myocytes by diffusion

The rate constant for the efflux of Ca^{2+} from permeabilized cardiomyocytes was estimated by examining the rate of decay of the Ca^{2+} signal after rapid application of caffeine/thapsigargin. Under these conditions, it was assumed that the

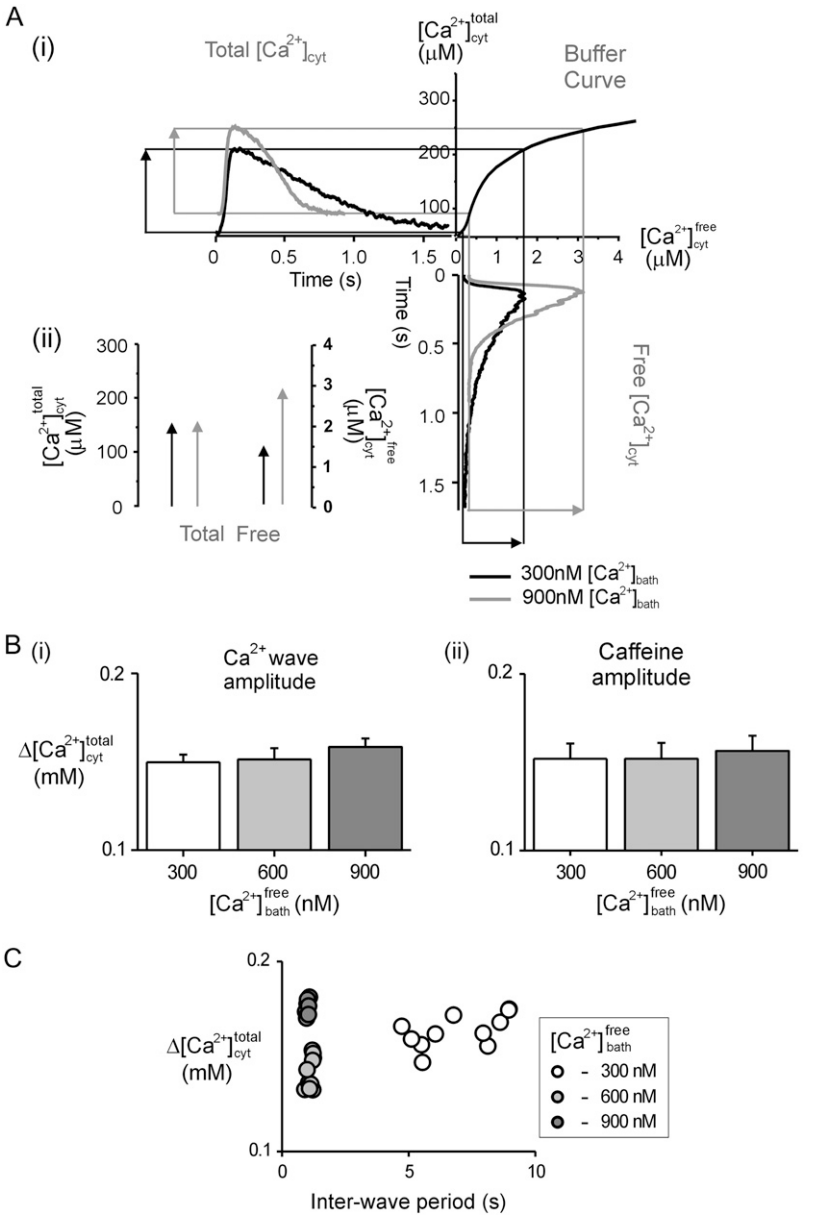

FIGURE 3 (*i*) Illustration of the conversion of $[Ca^{2+}]^{free}_{cyt}$ signals to $[Ca^{2+}]^{total}_{cyt}$ signals using the steady-state Ca^{2+} buffer curve. The Ca^{2+} transients are the average of eight Ca^{2+} sequential velocity-corrected Ca^{2+} waves at 320 nM (*black line*) and 880 nM (*gray line*). The buffer curve is based on published data (20). The arrows indicate the amplitudes of the Ca^{2+} waves both in terms of $[Ca^{2+}]^{free}_{cyt}$ and $[Ca^{2+}]^{total}_{cyt}$. (*ii*) Amplitude of the Ca^{2+} wave at both 320 and 880 nM in terms of $[Ca^{2+}]^{total}_{cyt}$ (*right-hand side*) and $[Ca^{2+}]^{free}_{cyt}$ (*left-hand side scale*). (*B* (*i*)) Mean values of the amplitude of Ca^{2+} wave at a range of $[Ca^{2+}]^{free}_{bath}$ values expressed in terms total $[Ca^{2+}]_{cyt}$. (*ii*) Mean values of caffeine transient amplitude at a range of $[Ca^{2+}]^{free}_{bath}$ values.

rate of decay of the Ca^{2+} signal was dependant on the loss of Ca^{2+} from the permeabilized cell by diffusion. The method used to estimate the rate of diffusion is illustrated in Fig. 4, the decay of $[Ca^{2+}]^{free}_{cyt}$ within the cell was converted to a $[Ca^{2+}]^{total}_{cyt}$ signal as described in Fig. 3 *A*. The resultant signal was fitted a polynomial (fourth to eighth order) to obtain a smoothed $[Ca^{2+}]^{total}_{cyt}$ decay curve. The polynomial fit of the decay time course was differentiated (to calculate Ca^{2+} flux) and plotted against the corresponding $\Delta[Ca^{2+}]^{free}_{cyt}Z$ signal ($[Ca^{2+}]^{free}_{cyt} - [Ca^{2+}]^{free}_{bath}$). As shown in Fig. 4 *B*, this relationship was approximately linear, the gradient of which reflected the value of the rate constant to describe the loss of Ca^{2+} from the cell. The average rate constant was 30.1 ± 2.1 s^{-1} ($n = 24$ cells). Knowledge of this constant allowed the $[Ca^{2+}]^{total}_{cyt}$ signal to be corrected for the Ca^{2+} loss and gain from the extracellular space during the Ca^{2+} wave. An example of the corrected transient is shown in Fig. 4 *C* and the signal represents the total Ca^{2+} released and taken up by the SR during a single Ca^{2+} wave. Despite the high $[Ca^{2+}]^{free}_{cyt}$ during a wave, the loss of Ca^{2+} from the cell by diffusion is small, at the peak of the transient it is ~3 μM, and by the end of the transient the value is ~10 μM compared to the total released from the SR of ~150 μM.

Estimation of the background leak of Ca^{2+} from the SR

Ca^{2+} efflux from the cardiac SR in the absence of Ca^{2+} waves is thought to be mainly due to spontaneous non-propagating Ca^{2+} sparks that generate a background Ca^{2+}

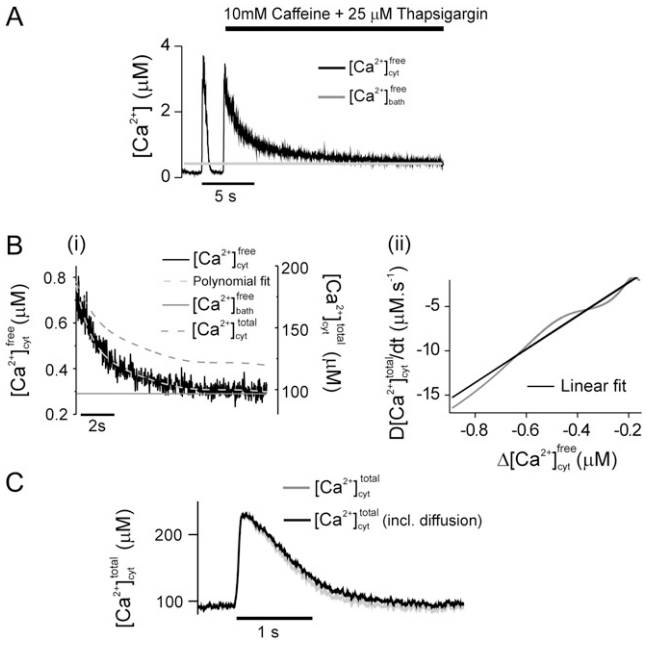

FIGURE 4 (*A*) Records of $[Ca^{2+}]^{free}_{cyt}$ and $[Ca^{2+}]^{free}_{bath}$ derived from the average fluorescence measured from a 20-pixel average of a continuous line-scan image. After a Ca^{2+} wave, caffeine (10 mM) and thapsigargin (25 μM) were rapidly applied. Panel *B* shows the decay phase of the Ca^{2+} signal in caffeine and thapsigargin on an expanded timescale. The light gray dashed line is the fourth-order polynomial fit to decay phase. The dark gray dashed line is the $[Ca^{2+}]^{total}_{cyt}$ signal derived from the standardized Ca^{2+} buffer curve. (*B* (*ii*)) Plot of the $\Delta[Ca^{2+}]_{cyt}$ signal ($[Ca^{2+}]^{free}_{cyt} - [Ca^{2+}]^{free}_{bath}$) derived from the (polynomial fitted signals) and the time derivative of the $[Ca^{2+}]^{total}_{cyt}$ signal (*gray line*). The black line represents the best fit linear relationship to the function. The slope of this relationship is the rate constant for the diffusion of Ca^{2+} from the cardiomyocyte (40 $\pm$ 2 s^{-1}). The application of this rate constant to the $[Ca^{2+}]^{total}_{cyt}$ signal predicts the change in total $[Ca^{2+}]^{total}_{cyt}$ within the cytosol including the gain and loss of Ca^{2+} by diffusion. These two signals are shown in panel *C*.

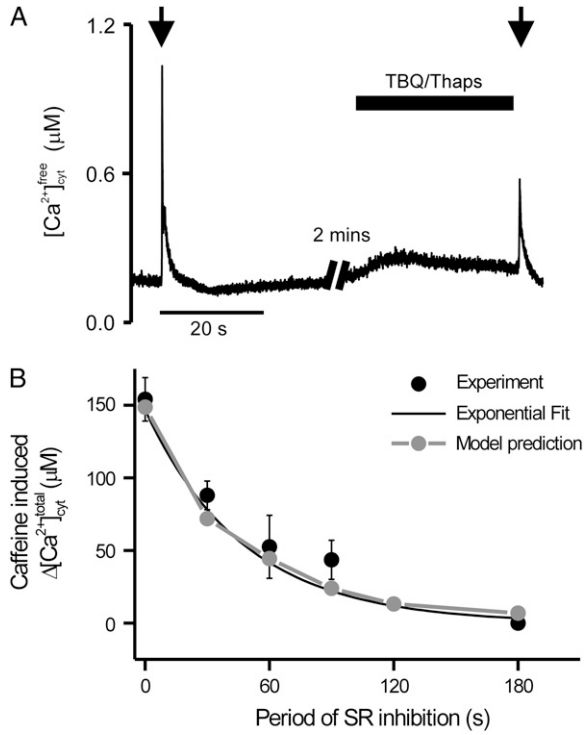

FIGURE 5 (*A*) An example of the protocol used to determine the rate of loss of Ca^{2+} from the SR, plot of $[Ca^{2+}]^{free}_{cyt}$ signal derived from a 20-pixel average of a line-scan image of a permeabilized cardiomyocyte perfused with 150 nM Ca^{2+} (300 μM EGTA, 10 μM Fluo-5). Caffeine (10 mM) was briefly applied at the times shown by the arrows. The cardiomyocyte was perfused for a further 2 min after the initial caffeine exposure to ensure reequilibration of the SR. Thapsigargin (25 μM) and 50 μM cyclopiazonic acid (CPA) was perfused continuously for a range of times (30, 60, 90, 120 and 180 s) before the second application of caffeine. (*B*) Plot of the mean ($\pm$ SE) of the amplitude of caffeine-induced Ca^{2+} release (converted to $[Ca^{2+}]^{total}_{cyt}$) versus incubation time in TBQ/thapsigargin (●). The solid black line is the best fit single exponential decay to the data. Computational modeling using the rate constant for SR Ca^{2+} leak predicted a decrease in Ca^{2+} transient amplitude shown by gray line with gray circle.

leak from the SR. The magnitude of the background flux can be quantified by monitoring the loss of Ca^{2+} from the SR in the absence of SERCA activity. These measurements were made in permeabilized cardiomyocytes as shown in Fig. 5 *A*. Cells were perfused with $[Ca^{2+}]^{free}_{bath}$ of 150 nM in the presence of 0.3 mM EGTA. Rapid and complete inhibition of SERCA was achieved by using a mixture of two SERCA inhibitors, 2′,5′-di(tert-butyl)-1,4-benzohydroquinone (TBQ) (25 μM) and thapsigargin (25 μM). The time course for the loss of SR Ca^{2+} was tracked by application of 10 mM caffeine at fixed times after SERCA inhibition. The amplitude of the $[Ca^{2+}]^{total}_{cyt}$ signal at each time point was taken to reflect the SR Ca^{2+} content. Fig. 5 *B* shows the mean data from a number of experiments, the time course of the decay suggests an approximately exponential decay of SR Ca^{2+} content with a rate constant of 1.37 $\pm$ 0.01 min^{-1} ($n = 8$ cells). The additional curve shown in Fig. 5 *B* is the predicted time course of the decrease in amplitude of caffeine-induced Ca^{2+} signals from the computational model described below.

Calculation of SERCA-mediated fluxes from the time course of the Ca^{2+} wave

Fig. 6 illustrates the approach used to estimate the SERCA-mediated flux and subsequently the time course and magnitude of RyR2-mediated Ca^{2+} flux during a Ca^{2+} wave. Fig. 6, *A* and *B*, show the time course of the change in $[Ca^{2+}]^{free}_{cyt}$ and $[Ca^{2+}]^{total}_{cyt}$ (corrected for diffusion), respectively, during a Ca^{2+} wave. A smoothed waveform of the $[Ca^{2+}]^{total}_{cyt}$ signal was generated by a pair of fourth- to eighth-order polynomials fitted to the upstroke and decay phases of the waveform (*gray line*). The net Ca^{2+} flux associated with a Ca^{2+} wave was calculated by differentiating the $[Ca^{2+}]^{total}_{cyt}$ signal to generate the waveforms shown in Fig. 6 *C* (*back line*). The differential of the polynomial fit generated a smooth time course (*gray line*), whereas the magnitude of the release phase (positive flux) could be resolved directly from the Ca^{2+} signal. But the differential of the original total Ca^{2+}

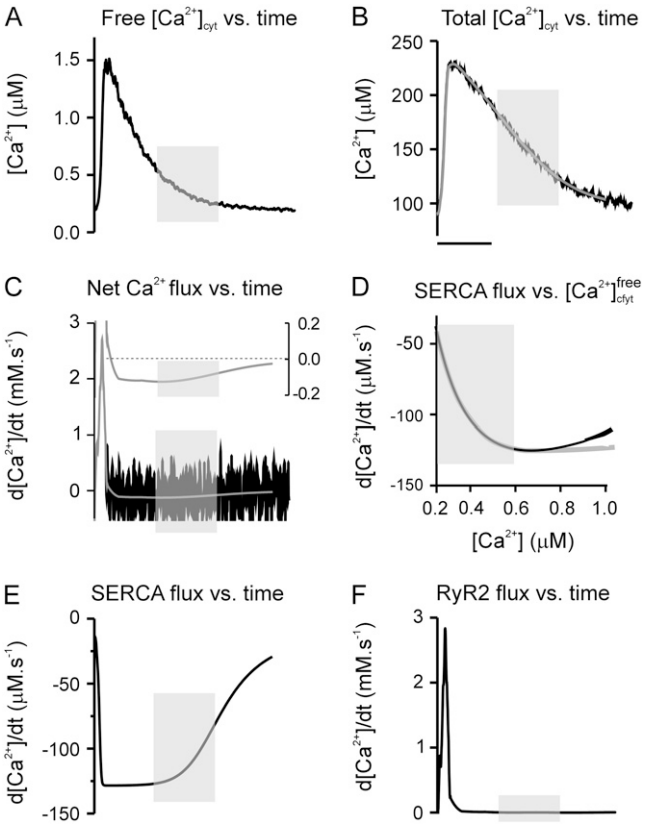

FIGURE 6 Illustration of the methods used to derive the parameters associated with SERCA-mediated Ca^{2+} uptake and RyR2-mediated Ca^{2+} release. (*A*) The time course of the $[Ca^{2+}]_{cyt}^{free}$ signal measured from a permeabilized cardiomyocyte perfused with $[Ca^{2+}]_{bath}^{free} \sim 300$ nM Ca^{2+}. The signal is derived from the average of eight sequential Ca^{2+} waves, 20 pixels wide, and corrected for wave velocity. The gray shaded area marks the region of the trace from which the SERCA parameters are derived (*D*). (*B*) The corresponding diffusion-corrected $[Ca^{2+}]_{cyt}^{total}$ signal (*black line*) and the superimposed two-part, fourth-order binomial fit to the transient (*gray line*). (*C*) The time differential of the $[Ca^{2+}]_{cyt}^{total}$ signal ($d[Ca^{2+}]/dt$) shown in panel *B* (*black line*); the time differential of the binomial fit is shown by the gray line. The inset shows the lower section of the plot at an expanded scale. (*D*) Plot of the rate of change of $[Ca^{2+}]_{cyt}^{total}$ (against the corresponding $[Ca^{2+}]_{cyt}^{free}$ signal (*black line*)); the gray rectangle is the region of plot used to derive the SERCA parameters of H_f, K_{mf}, and V_{max} (20). (*E*) Plot of the predicted SERCA activity throughout the Ca^{2+} wave based on the values of $[Ca^{2+}]_{cyt}^{free}$ and the SERCA parameters derived in panel *D*. (*F*) The Ca^{2+} efflux time course calculated by subtraction of the SERCA flux from the total Ca^{2+} flux signal.

signal was too noisy to extract the negative flux (uptake phase) of the signal. The time course of the negative phase was resolved from the differential of a polynomial fit (*inset*, Fig. 6 *C*). During the latter phase of these signals (the section highlighted by the *gray area*), the underlying Ca^{2+} fluxes were assumed to be: i), background SR Ca^{2+} leak (Fig. 4); ii), diffusional loss/gain of Ca^{2+} (Fig. 3); and iii), SERCA-mediated Ca^{2+} flux. The rate constants associated with fluxes i and ii were estimated from the measurements described above and used to calculate the magnitude of the associated fluxes during the decay phase of the Ca^{2+} wave. These fluxes were subtracted from the underlying Ca^{2+} signal to reveal the SERCA-mediated flux (*black line*, Fig. 6 *D*). As shown in Fig. 6 *D*, between 200 and 600 nM $[Ca^{2+}]_{cyt}^{free}$, the relationship between the SERCA-mediated Ca^{2+} flux and the corresponding $[Ca^{2+}]_{cyt}^{free}$ fitted well with a previously published model of SERCA function (*gray line*; Appendix, Eq. A1) (20) and this allowed the estimate of the maximum turnover rate (V_{max}) and the Ca^{2+} sensitivity (K_{mf}) and slope (H) of SERCA. Once established, these values were assumed to apply for the complete time period of the Ca^{2+} wave (Fig. 6 *E*). These calculations suggested that for the majority of the time course of the Ca^{2+} wave, SERCA was operating at, or close to, the V_{max}.

Calculation of RyR2-mediated fluxes from the time course of the Ca^{2+} wave

By assuming that the calculated SERCA parameters and the rate constants for both background SR Ca^{2+} leak and the Ca^{2-}diffusion apply equally to the initial phase of the Ca^{2+} wave, the time course and magnitude of transient increase in RyR2-mediated Ca^{2+} flux can be estimated (Fig. 6 *F*). This approach predicted an RyR2-mediated efflux that peaks at $\sim$4 mMs^{-1} within 30 ms and decays to negligible values within 100 ms. The time course of the Ca^{2+} flux can be converted to a permeability by calculation of the corresponding changes in $[Ca^{2+}]_{SR}^{free}$ using previously published estimates of SR volume and intrinsic cellular buffering properties (22). This parameter is independent of the *trans*-SR Ca^{2+} concentration gradient and indicates the time course of the change in RyR2 activity. These calculations suggest that the Ca^{2+} efflux from the SR increases from a basal level of $\sim$1.2 μM/s to $\sim$3 mM/s during a Ca^{2+} wave as a result of a transient increase in the permeability of the SR to Ca^{2+}.

Derivation of SERCA flux and RyR2 flux parameters from Ca^{2+} waves generated at a range of intracellular [Ca^{2+}]

The analysis described in Fig. 6 was applied to Ca^{2+} waves recorded from cardiomyocytes exposed to solutions with a $[Ca^{2+}]_{bath}^{free}$ of $\sim$300, $\sim$600, or $\sim$900 nM Ca^{2+}. As shown in Fig. 7, the mean values of SERCA V_{max} and K_{mf} were not constant across this range of $[Ca^{2+}]_{bath}^{free}$; both increased significantly, whereas the change in slope (H) was not significant. The corresponding changes in RyR2 flux parameters predicted by the analysis are shown in Fig. 7, *A* (*iii*) and C. The calculated peak RyR2-mediated flux and permeability progressively increased over the range of [Ca^{2+}] studied but the duration at half-maximum (FWHM) was unchanged (Fig. 7 *C* (*iii*)).

Comparison of model and recorded Ca^{2+} wave parameters

The complete set of Ca^{2+} flux parameters for Ca^{2+} waves recorded in a typical permeabilized cell at $[Ca^{2+}]_{bath}^{free}$ of

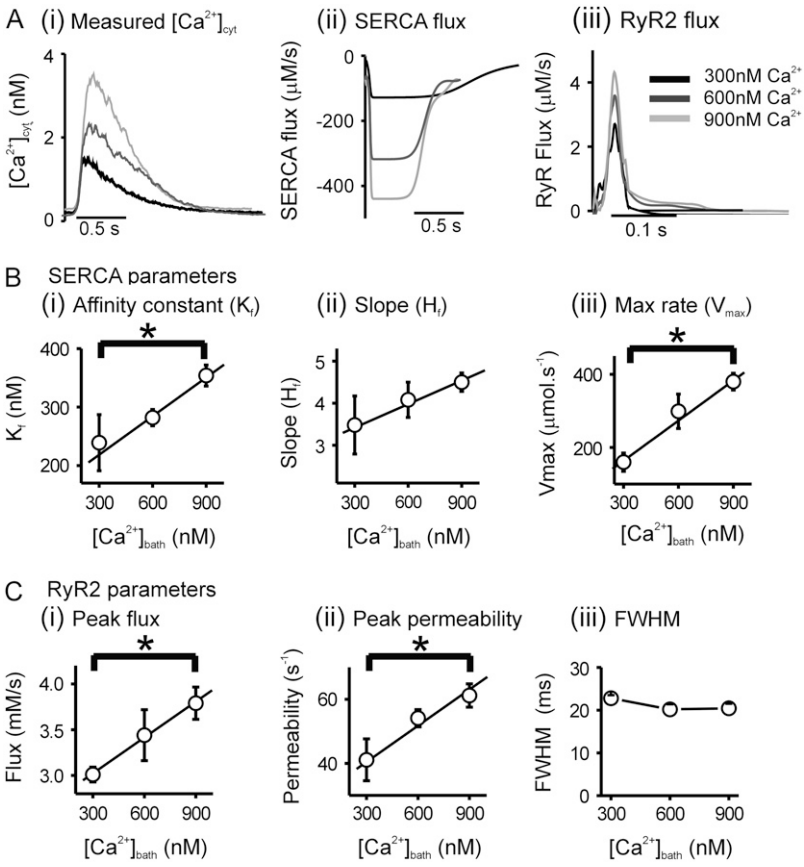

FIGURE 7 (*A* (*i*)) Superimposed Ca^{2+} waves measured at three different $[Ca^{2+}]_{bath}^{free}$. (*A* (*ii*)) Calculated SERCA flux from the three transients; (*A* (*iii*)) calculated RyR fluxes. (*B*) Average SERCA parameters extracted from Ca^{2+} waves recorded from eight to 10 rabbit ventricular myocytes at each $[Ca^{2+}]_{bath}^{free}$: (*i*) SERCA Ca^{2+} affinity constant (K_f); (*ii*) slope factor (H_f); (*iii*) maximum turnover rate (V_{max}). (*C*) Average RyR2 parameters extracted from Ca^{2+} waves recorded from eight to 10 rabbit ventricular myocytes at each $[Ca^{2+}]_{bath}^{free}$: (*i*) peak flux; (*ii*) peak permeability; (*iii*) fullwidth at half the maximal value (*FWHM*) of the change in peak permeability. Straight line is the best fit linear correlation to the data. $*p < 0.05$.

~300 nM (including the time course of RyR2-mediated Ca^{2+} flux) were used in a computational model to predict the time course and frequency of Ca^{2+} waves. The details of the model are given in the Methods section and in the Appendix, the only assumption used in the model is that RyR2-mediated Ca^{2+} release was triggered by the $[Ca^{2+}]_{SR}^{free}$ reaching a threshold value ($[Ca^{2+}]_{SR}^{threshold}$). This value was taken as the maximum free intra-SR [Ca^{2+}] calculated from the estimated total SR Ca^{2+} content. As shown in Fig. 8, the computational model predicted Ca^{2+} waves of similar time course (Fig. 8 *A*) and frequency to that observed experimentally. When run continuously to reach a steady state, the model generated Ca^{2+} transients at $[Ca^{2+}]_{bath}^{free} = 300$ nM that had a frequency, maximum and minimum $[Ca^{2+}]_{cyt}^{free}$ that was within 5% of the experimental data. The application of caffeine/thapsigargin was simulated by increasing background leak by a factor of 1000 and reducing V_{max} of SERCA by 1000. The resultant Ca^{2+} transient decayed with a similar time course to that observed experimentally due to loss of Ca^{2+} by diffusion. The calculated $[Ca^{2+}]_{SR}^{free}$ signal is shown to indicate the predicted time course of $[Ca^{2+}]_{SR}^{free}$ during release and loading to a threshold level during each wave. The third signal is the integral Ca^{2+} flux due to diffusion. This indicates that during each Ca^{2+} wave ~10 μmol of Ca^{2+} leaves the cell during the Ca^{2+} wave. In the period between Ca^{2+} waves, the same amount of Ca^{2+} enters the permeabilized cell from the extracellular space. Thus, in the steady state, the amount of Ca^{2+} leaving and entering the cell is balanced. Fig. 8 *B* (*i* and *ii*) show model predictions of Ca^{2+} waves at 900 nM Ca^{2+} under two conditions: i), with the same values of V_{max}, K_{mf}, H, and peak RyR2 permeability used to simulated waves at 300 nM; and ii), with the values of V_{max}, K_{mf}, and RyR2 peak permeability appropriate for 900 nM derived from the relationships shown in Fig. 7. As shown, without changing the SERCA and RyR2 values, the model predicts a rise of Ca^{2+} wave frequency (to 372% of control) and amplitude (to 136% of control). However, adjusting of the SR parameters to those appropriate for 900 nM predicts waves of higher frequency (514% of control) and similar amplitude (138%). The predicted increase in wave frequency going from 300 to 900 nM (514%) is comparable to that observed experimentally (481 $\pm$ 12%, $n = 10$). The same result can be achieved by using the SR parameters at 900 nM as the starting conditions and predicting the Ca^{2+} waves at 300 nM, the decrease in frequency of Ca^{2+} waves predicted by uncorrected SR parameters is less than that seen experimentally (data not shown). In summary, the use of fixed SERCA and RyR2 parameters to predict Ca^{2+} wave characteristics does not mimic the experimental data over a range of $[Ca^{2+}]_{bath}^{free}$. Adjustment of SERCA K_{mf} and V_{max} and

RyR2 maximum permeability is necessary to accurately predict changes Ca^{2+} wave frequency at different values of $[Ca^{2+}]^{free}_{bath}$.

The effects of CaM kinase inhibitor AIP on Ca^{2+} waves

One mechanism that may be responsible for the experimentally observed change in the characteristics of RyR2 and SERCA at different $[Ca^{2+}]^{free}_{cyt}$ is modulation of the activity of these proteins by phosphorylation via the Ca^{2+} sensitive enzyme CaM kinase (23). To test this hypothesis, intact cells were incubated with the CaM kinase inhibitor AIP before exposure to solutions containing either ~300 or ~600 nM Ca^{2+}. The data shown in Fig. 9 summarizes the Ca^{2+} wave characteristics and the derived SERCA and RyR2 parameters relative to those measured at $[Ca^{2+}]^{free}_{bath} = 300$nM. Incubation with AIP reduced the degree to which the Ca^{2+} wave frequency increased at $[Ca^{2+}]^{free}_{bath} = 900$ nM (from 481 ± 12%, $n = 10$ to 340 ± 10%, $n = 15$, $P < 0.05$; Fig. 9 *A* (*iii*)) but did not change any other aspect of the Ca^{2+} wave (Fig. 9 *A* (*i* and *ii*)). Analysis of Ca^{2+} fluxes indicated that AIP treatment prevented the apparent increase in SERCA V_{max} observed at 900 nM Ca^{2+} ($P < 0.05$; Fig. 9 *B* (*iii*)) but the effect of AIP on SERCA K_{mf} and H were not statistically different from the control values. Furthermore, the derived values of peak RyR2 flux and permeability after AIP treatment were significantly lower than control values at 900 nM $[Ca^{2+}]^{free}_{bath}$ ($P < 0.05$). Wave velocity in AIP was significantly lower after AIP treatment (130 ± 7 μm/s) compared to control (180 ± 5 μm/s), and was similar to that measured at $[Ca^{2+}]^{free}_{bath} = 300$ nM (130 ± 4 μm/s). AIP treatment did not significantly affect any of the Ca^{2+} wave parameters or derived SERCA and RyR2 parameters at $[Ca^{2+}]^{free}_{bath} = 300$nM. Plotted on the right-hand side of each on the panels in Fig. 9 are the relative changes in parameters on raising $[Ca^{2+}]^{free}_{bath}$ from 300 to 900 nM predicted by the computational model under two conditions: i), with values of SERCA and RyR2 values corrected for increased $[Ca^{2+}]$; and ii), using values of SERCA and RyR2 parameters appropriate for $[Ca^{2+}]^{free}_{bath} = 300$nM. The effects of removing Ca^{2+} correction on i), Ca^{2+} wave frequency; ii), SERCA turnover rate (V_{max}); and iii), RyR2 peak permeability is similar to that observed experimentally on addition AIP. This supports the view that AIP inhibits the Ca^{2+}-dependent changes in SERCA and RyR2 function observed upon raising the $[Ca^{2+}]^{free}_{bath}$ from 300 to 900nM.

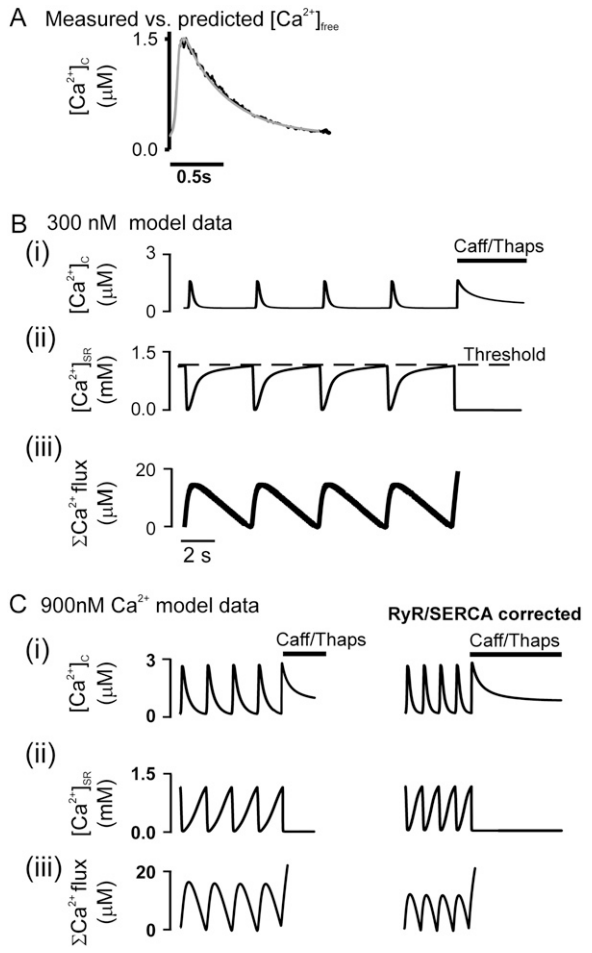

FIGURE 8 Sample data from the computational model of Ca^{2+} waves. (*A*) Using the experimentally measured values of the various fluxes underlying a Ca^{2+} wave, the signal was recreated (*gray line*) and superimposed on the experimentally recorded signal (*black line*) recorded at $[Ca^{2+}]^{free}_{bath} =$ 300nM. (*B*) The computational model was run continuously for 10 s, the $[Ca^{2+}]^{threshold}_{SR}$ was calculated from the experimentally measured total SR Ca^{2+} content. At the point indicated, caffeine/thapsigargin was simulated by increasing background leak by 1000× and decreasing SERCA V_{max} by 1000×. Model data for (*i*) $[Ca^{2+}]^{free}_{cyt}$; (*ii*) $[Ca^{2+}]^{free}_{SR}$; (*iii*) net Ca^{2+} flux. (*C*) Model data for Ca^{2+} waves at $[Ca^{2+}]^{free}_{bath} = 900$nM, (*i*) $[Ca^{2+}]^{free}_{cyt}$; (*ii*) $[Ca^{2+}]^{free}_{SR}$; (*iii*) net Ca^{2+} flux. On the right-hand side, the model output after correction of RyR and SERCA parameters for raised $[Ca^{2+}]^{free}_{bath}$ according to the relationships shown in Fig. 7.

DISCUSSION

This study examines in detail the characteristics of Ca^{2+} waves in cardiomyocytes at a range of cellular Ca^{2+} loads. The data indicate that a fixed amount of Ca^{2+} is released from the SR across a range of cellular $[Ca^{2+}]$ values; locally the amount released is comparable to that release by high caffeine/thapsigargin application suggesting that a Ca^{2+} wave causes almost complete depletion of the SR. Estimates of the underlying Ca^{2+} fluxes during a Ca^{2+} wave indicates that the peak fluxes associated with SERCA and RyR2 activity are modulated by the average $[Ca^{2+}]^{free}_{cyt}$. These changes can be prevented by inhibition of CaM kinase using the peptide AIP. The flux data were used to create a computational model of cardiac SR that accurately predicts the time course and frequency of Ca^{2+} release from the SR across a range cellular Ca^{2+} loads. The model quantifies the change in Ca^{2+} wave parameters expected if the relative

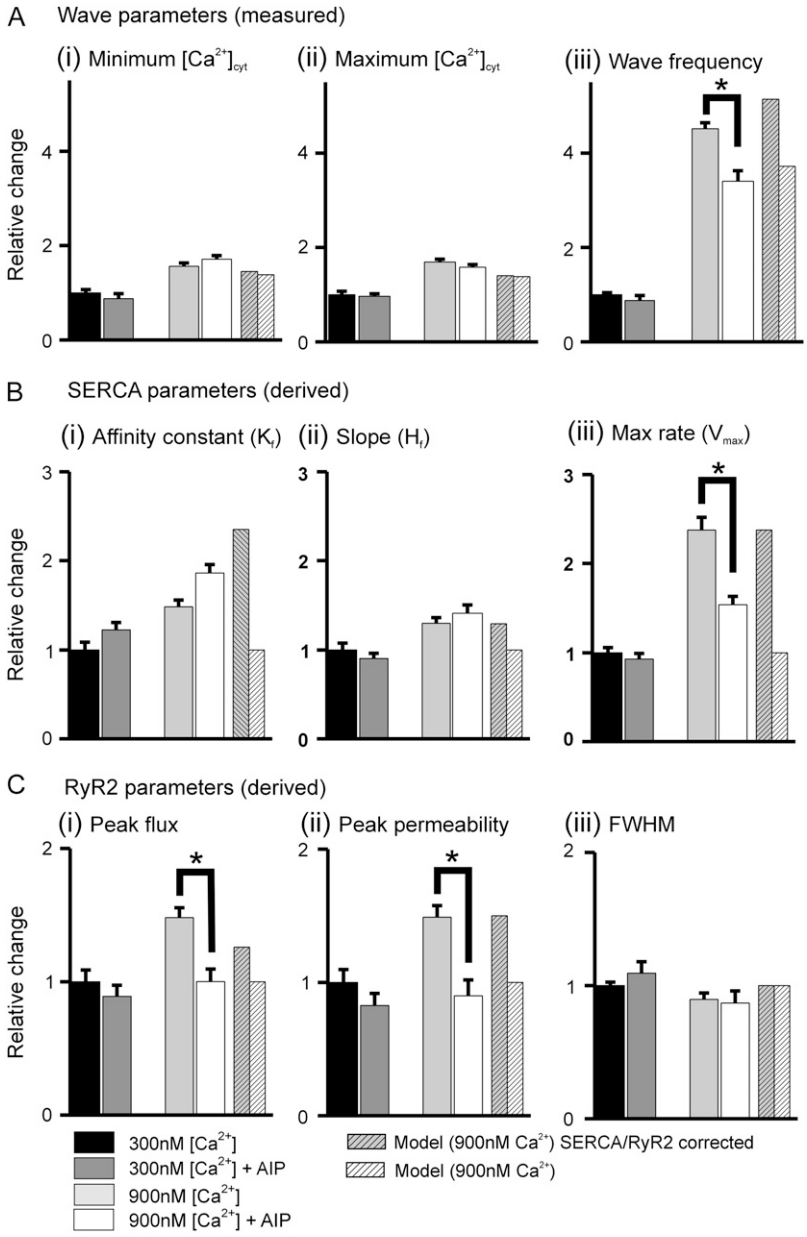

FIGURE 9 Relative change in measured (*A*) and derived (*B* and *C*) Ca^{2+} wave parameters at 900 nM relative to those at 300 nM before and after treatment with the CaM kinase II inhibitor AIP (see key). (*A* (*i*)) Minimum $[Ca^{2+}]_{cyt}^{free}$; (*ii*) maximum $[Ca^{2+}]_{cyt}^{free}$; (*iii*) wave frequency. Hatched bars represent the relative change in wave parameters calculated by the computational model with and without the correction for changes in RyR and SERCA. (*B*) Relative change in SERCA parameters (*i*) K_f, (*ii*) slope (H_f), and (*iii*) maximum turnover rate (V_{max}). (*C*) Calculated RyR parameters (*i*) peak flux, (*ii*) peak permeability, and (*iii*) the fullwidth at half the maximal change in permeability (*FWHM*).

fluxes via RyR2 and SERCA were to remain constant. This is interesting because these calculations indicate that the moderate reduction of Ca^{2+} wave frequency observed at $[Ca^{2+}]_{bath}^{free} = 900$ nM after AIP treatment does not result from the incomplete action of the drug. This effect is consistent with the anticipated effects of removing the Ca^{2+} sensitivity of the SR uptake and release parameters.

Comparison between Ca^{2+} wave and caffeine transient

Careful calibration of fluorescence signals allowed the accurate measurement of $[Ca^{2+}]_{cyt}^{free}$ within a limited region of the cytosol of permeabilized cardiac cells (11). Previous studies have shown that both intact and permeabilized cells exhibit a threshold $[Ca^{2+}]_{cyt}^{free}$ for Ca^{2+} wave generation of above ~200 nM. Above this value, cycles of spontaneous SR Ca^{2+} release occur with increasing frequency as the cellular Ca^{2+} load is increased. At the whole cell level, spontaneous Ca^{2+} release was estimated to deplete the SR Ca^{2+} by ~15% compared to that achieved during rapid application of caffeine (7). This study suggests that Ca^{2+} release during a fully propagating Ca^{2+} wave locally depletes the SR by ~100% compared to that achieved by caffeine. This observation is not contrary to the measurements from intact cardiac myocytes; normally the complete Ca^{2+} wave takes ~1 s to propagate along the length of the cell at room temperature. But at any one time over this period

only ~20% of the volume of the cardiomyocyte experiences an increased $[Ca^{2+}]_{cyt}^{free}$; ~80% of the volume is either awaiting the arrival of the Ca^{2+} wave or is recovering after the release phase. In contrast, caffeine releases Ca^{2+} synchronously throughout the cardiomyocyte; therefore local and whole cell signals are comparable. A similar principal applies to the published records of luminal Ca^{2+} using Fluo-5N fluorescence. These data suggest that a Ca^{2+} wave releases ~60–70% of the total caffeine-accessible signal (24,25). These studies may have underestimated the amplitude of signal associated with a Ca^{2+} wave. The Fluo-5N line-scan signal of a Ca^{2+} wave was derived from the average fluorescence from the full length of the cell. The finite time (~1 s) for the wave to propagate along the length of the cell will smear the time course and reduce the amplitude of the signal. A similar phenomenon is seen with the Fluo-5F cytoplasmic signals (see Supplementary Fig. 3). This averaging of the nonsynchronous Ca^{2+} wave signal may explain why the amplitude is lower than those observed with synchronous caffeine-induced signals.

The data described in this study are entirely derived from permeabilized cardiac myocytes, but the principles are thought to apply to Ca^{2+} waves in intact myocytes. Previous studies have compared intact and permeabilized cells; no significant differences were observed in time course, amplitude, or frequency of spontaneous Ca^{2+} waves recorded from these two preparations (10,26).

Raising the cellular Ca^{2+} load increased the minimum and maximum $[Ca^{2+}]_{cyt}^{free}$ and apparently increased the amplitude of $[Ca^{2+}]_{cyt}^{free}$ change during the Ca^{2+} wave. However, when the total Ca^{2+} released from the SR at various cellular Ca^{2+} loads was calculated the increase in $[Ca^{2+}]_{cyt}^{total}$ within the cytosol during a Ca^{2+} wave was constant (~0.15 mM) regardless of the cellular Ca^{2+} load (Fig. 3 *C*). This calculation and the subsequent analysis is based on the assumption that the only subcellular components contributing to the intracellular Ca^{2+} signals are: i), cytoplasmic Ca^{2+} buffers; ii), SR Ca^{2+} release and uptake processes; iii), intra-SR Ca^{2+} buffers. There is evidence that cardiac mitochondria contribute to Ca^{2+} homeostasis (27,28), but previous work indicates that under the conditions of this study, the activity of mitochondria does not influence the time course or frequency of the Ca^{2+} waves (11).

Measurement of background Ca^{2+} fluxes

The rate constant for Ca^{2+} loss from a permeabilized cardiomyocyte was calculated from the rate of decay of the caffeine-induced response. Assuming this value can be applied to Ca^{2+} movement both into and out of the myocyte, this was used to calculate the magnitude of Ca^{2+} fluxes across the permeabilized membrane during a Ca^{2+} wave. These calculations suggested that only a small amount of Ca^{2+} is lost and gained during a Ca^{2+} wave cycle (~10 μM) compared to the total released from the SR (~150 μM). Interestingly, these estimates are close to those published for intact cardiomyocytes where Ca^{2+} loss and gain from the cell is via sarcolemmal transport processes (mainly the Na^+/Ca^{2+} exchange) (7).

In a separate set of experiments, the efflux of Ca^{2+} from the SR in the absence of Ca^{2+} waves was estimated by monitoring the decline in SR Ca^{2+} content at various times after rapid inhibition of SERCA. This time course was approximately exponential and could be adequately modeled with a single rate constant. This was used to estimate the rate of efflux of Ca^{2+} from the SR in the periods between Ca^{2+} waves; a flux that is normally countered by the activity of SERCA. Over the initial 30 s after inhibition of SERCA, the leak of Ca^{2+} from the SR was ~1.2 μM/s. This value is lower than those measured in intact rabbit myocytes using rapid tetracaine application (4–15 μM/s) (22) but higher than estimates in earlier studies (20,29). One possibility for the range of values is the critical dependence of leak rate on SR luminal Ca^{2+}, a variable that was not necessarily constant across studies.

Model derived values of SERCA and RyR2 fluxes

Assuming that the transient increase in SR Ca^{2+} permeability that caused the Ca^{2+} wave did not contribute significantly to the Ca^{2+} signal late on in the decay phase of the wave, then the Ca^{2+} fluxes determining the $[Ca^{2+}]_{cyt}^{free}$ in the latter part of the wave are: i), exchange with the bath solution; ii), background efflux from the SR; and iii), uptake by SERCA. Since i and ii are known, iii was calculated using a previously published model of SERCA (20). The values of SERCA binding constant (200–300 nM), the slope of the relationship (3–4), and the maximum turnover rate (V_{max}) values (200–400 μM/s) are comparable to those values estimated for the intact cardiac myocyte (20,22,30). When these SERCA characteristics were used to predict SERCA activity early in the Ca^{2+} wave it was clear that, for the majority of the release phase, SERCA will be operating at maximal turnover rate. Assuming that SERCA activity can influence the Ca^{2+} signal immediately (~5 ms) after the release of Ca^{2+} from the SR, the predicted SERCA fluxes during the Ca^{2+} wave were used to predict the corresponding SR Ca^{2+} release waveform required to generate the measured change in $[Ca^{2+}]_{cyt}^{free}$. The transient rise of SR flux calculated by this approach peaked within 30 ms with a flux rate of ~2–3 mM/s and was complete by ~100 ms. These values are comparable to those measured during E-C coupling in cardiomyocytes at high SR Ca^{2+} loads (31–33). Throughout these calculations, equilibrium constants and not rate constants were used to calculate Ca^{2+} binding to cytosolic buffers and SERCA. This simplifying assumption has been made by several previous studies (20,34–36) and is justified in the current study by the relatively coarse spatial (~5 μm) and temporal resolution (10 ms) of the measurements.

Changes in Ca^{2+} wave characteristics with cellular [Ca^{2+}]

Examination of the characteristics of the Ca^{2+} waves at a range of cellular [Ca^{2+}] revealed changes in the calculated underlying Ca^{2+} fluxes (Fig. 7, *B* and *C*). The analysis suggests that the time course of the Ca^{2+} wave at higher $[Ca^{2+}]^{free}_{bath}$ require changes in the parameters for both SERCA and the RyR2 activity. The most striking of these changes are the increase in SERCA V_{max} and the increased peak permeability of release waveform. This suggests that the increased frequency of the Ca^{2+} waves at higher cellular Ca^{2+} load cannot simply be explained by a fixed set of SR fluxes. This conclusion was confirmed using a computational model. Using the characteristics of the SR that apply at 300 nM to predict the changes in wave characteristics at 900 nM indicated an increase in Ca^{2+} wave frequency that was considerably lower than that observed (375 vs. 514%). Using the higher SERCA and RyR2 parameters measured at $[Ca^{2+}]^{free}_{bath} \sim 900$ nM reproduced the Ca^{2+} wave frequency to within 5% of the measured values (481 $\pm$ 12%).

Changes in Ca^{2+} wave velocity with cellular [Ca^{2+}]

Ca^{2+} wave velocity was higher when the $[Ca^{2+}]^{free}_{bath}$ and therefore the mean $[Ca^{2+}]^{free}_{cyt}$ was increased. A positive correlation between Ca^{2+} wave amplitude and velocity has been previously reported for propagated waves in intact (37) and permeabilized cardiomyocytes (10,11). Although the precise mechanism underlying the relationship has not been verified, propagation of a Ca^{2+} wave is thought to be mediated via a ''fire-diffuse-fire'' mechanism between discrete clusters of RyR (14,38,38). Simplistically, larger Ca^{2+} release would be expected to propagate faster because the threshold $[Ca^{2+}]^{free}_{cyt}$ required to trigger release at adjacent sites would be attained earlier. A computational model of Ca^{2+} waves in the heart (14) indicated that over a limited range of wave amplitudes, an approximately linear relationship existed between Ca^{2+} wave propagation velocity (v) and the coefficient σ/dc^* where d is the distance between release sites, c^* is the threshold $[Ca^{2+}]^{free}_{cyt}$ for Ca^{2+} release, and σ is the amount of Ca^{2+} released from the SR (14). Normally, the parameters d and c^* are considered fixed, but modeling of Ca^{2+} waves has been extended to include an influence of luminal [Ca^{2+}] ($[Ca^{2+}]^{free}_{SR}$) on c^* (39). A considerable amount of data now supports the concept that increased SR luminal [Ca^{2+}] ($[Ca^{2+}]^{free}_{SR}$) acts on luminal sensors to increase the open probability of RyR2 and hence lower the cytoplasmic threshold for Ca^{2+} release (c^*) (39,40).

Recent work suggests that the SERCA activity between adjacent release sites may directly influence propagation velocity (41). In particular, rapid inhibition of SERCA instantaneously reduced conduction velocity (42). This suggests that SERCA mediated uptake has a role in the propagation of the Ca^{2+} wave. In particular, the high $[Ca^{2+}]^{free}_{cyt}$ after release at one site may activate SERCA and increase $[Ca^{2+}]^{free}_{SR}$ in adjacent sites thereby lowering the cytoplasmic threshold for release (c^*). If this mechanism acted as a modulatory influence then factors that increase SERCA V_{max} would be anticipated to increase propagation velocity by increasing the rate of rise of $[Ca^{2+}]^{free}_{SR}$. The data presented in this study are consistent with this theory; the increased propagation velocity observed at higher $[Ca^{2+}]^{free}_{bath}$ was paralleled by an apparent increase in SERCA V_{max}. After inhibition of CaM kinase, neither the calculated SERCA V_{max} nor the propagation velocity was significantly increased at the higher $[Ca^{2+}]^{free}_{bath}$, despite an increase in Ca^{2+} wave amplitude.

CaM kinase inhibition

CaM kinase II is the most obvious candidate for the Ca^{2+}-dependent modulation of SERCA and RyR2 observed in this study. The enzyme exists both within the cytosol and bound to the SR membrane in cardiac muscle and has previously been reported to influence the activity of SERCA and RyR2 via phosphorylation (23). Support for this hypothesis was obtained by using the CaM kinase inhibitor AIP, which appeared to alter the Ca^{2+} wave characteristics at high $[Ca^{2+}]^{free}_{bath}$ (~900 nM), but not at lower values (~300 nM). Furthermore, flux analysis of Ca^{2+} waves suggests that the effects of CaM kinase inhibition could be explained by the preventing the increase in SERCA V_{max} and RyR2 peak permeability observed at $[Ca^{2+}]^{free}_{bath} = 900$ nM (Fig. 9). The increased values of SERCA V_{max} at higher $[Ca^{2+}]^{free}_{bath}$, reversed by CaM kinase inhibitors, is entirely consistent with previous reports of the effects of CaM kinase phosphorylation on SERCA (43). This contrasts with A-kinase mediated effects that change in the Ca^{2+} affinity of the pump.

In intact myocardium, frequency-dependent acceleration (FDA) of relaxation is an important part of the physiological response to increased frequency of stimulation. The role of CaM kinase in this response is controversial (44,45). The data in this study would suggest that a similar FDA of Ca^{2+} uptake occurs in spontaneously active cardiac cells. As the mean $[Ca^{2+}]^{free}_{cyt}$ is increased, the CaM kinase-mediated effect enhances SERCA activity and increases the frequency of spontaneous Ca^{2+} release.

Increasing $[Ca^{2+}]^{free}_{bath}$ also affected the Ca^{2+} efflux pathways. The marked increase in permeability observed at $[Ca^{2+}]^{free}_{bath} \sim 900$ nM was prevented by inhibition of CaM kinase by AIP treatment. Previous reports on the consequences of CaM kinase phosphorylation of RyR2 are controversial, with increases (46) and decreases (47) being reported. In mice overexpressing CaM kinase II, spark frequency approximately doubles (48), and the enhanced CaM kinase II activity in heart failure is linked to the increased leak via RyR2 in heart failure (49,50). The data in this study is consistent with CaM kinase mediated stimulation of

RyR2 activity. These effects combined with CaM kinase mediated effects on SERCA increase the frequency of spontaneous Ca^{2+} waves in cardiac muscle. At the higher cellular [Ca^{2+}] values that occur at high heart rates, the increased CaM kinase activation is unlikely to increase the probability of spontaneous Ca^{2+} release during diastole due to the corresponding shorter diastolic period. But the increased CaM kinase II expression and activity documented in failing hearts (49–52) may increase the probability of spontaneous Ca^{2+} release at normal heart rates, a potentially proarrhythmic event.

APPENDIX

SERCA-mediated Ca^{2+} flux

Estimates of SERCA activity was fitted to the equation containing parameters for forward and reverse modes (53).

$$J_{SR} = \frac{V_{max}([Ca^{2+}]_i/K_{mf})^H - V_{max}([Ca^{2+}]_{SR}/K_{mr})^H}{1 + ([Ca^{2+}]_i/K_{mf})^H + ([Ca^{2+}]_{SR}/K_{mr})^H}, \quad \text{(A1)}$$

where V_{max} = maximal pump rate, $[Ca^{2+}]_i$ = intracellular [Ca^{2+}], K_{mf} = forward Michaelis-Menten pump constant, K_{mr} = backward Michaelis-Menten pump constant, H = Hill coefficient, $[Ca^{2+}]_{SR}$ = intra-SR [Ca^{2+}], $K_{mr} = 7000 \times K_{mf}$.

Ca^{2+} diffusion between cytoplasm and extracellular space

$$J_{diff} = k \times ([Ca^{2+}]_{cyt}^{free} - [Ca^{2+}]_{bath}^{free}). \quad \text{(A2)}$$

Sarcolemmal diffusional flux (J_{diff}) was derived from the decline of $[Ca^{2+}]_{cyt}$ following caffeine-induced SR Ca^{2+} release. The declining phase was fitted with a high (fifth to eighth) order polynomial and converted to $[Ca^{2+}]_{cyt}^{total}$ using Eq. 4. The first derivative of this was then calculated, plotted against the *trans*-sarcolemmal Ca^{2+}. The gradient of this relationship gave the value k in Eq. 4.

Ca^{2+} leak from the SR during period between Ca^{2+} waves

Leak was calculated on the basis of SR-cytosol concentration gradient, with the equation below.

$$J_{leak} = k_{leak} \times ([Ca^{2+}]_{SR}^{free} - [Ca^{2+}]_{cyt}^{free}), \quad \text{(A3)}$$

where k_{leak} is calculated from data obtained in this study (1.37 ± 0.01 min^{-1}).

Cytoplasmic Ca^{2+} buffering

Ca^{2+} buffering in the cytosolic compartment was based on a previously derived values by Hove-Madsen and Bers (21) and described by the equation below:

$$[Ca^{2+}]_{cyt}^{free} = [Ca^{2+}]_{cyt}^{free} + \frac{B_{max(1)}}{[1 + (K_{b(1)}/[Ca^{2+}]_{cyt}^{free})]} + \frac{B_{max(2)}}{[1 + (K_{b(2)}/[Ca^{2+}]_{cyt}^{free})]}, \quad \text{(A4)}$$

where $B_{max(1)}$ and $B_{max(2)}$ are the maximum free buffer concentrations (68 μmol/kg wet wt and 86 μmol/kg wet wt), and $K_{b(1)}$ and $K_{b(2)}$ are the dissociation constant for each buffer (0.42 μM and 79 μM).

Intra-SR Ca^{2+} buffering

Intra-SR Ca^{2+} buffering was quantified using parameters derived from Shannon and Bers (20). The free [Ca^{2+}] within the SR ($[Ca^{2+}]_{SR}^{free}$) was calculated from $[Ca^{2+}]_{SR}^{total}$ as follows:

$$[Ca^{2+}]_{SR}^{free} = \frac{B_{max} \times [Ca^{2+}]_{SR}^{total}}{kd + [Ca^{2+}]_{SR}^{total}}. \quad \text{(A5)}$$

The Ca^{2+} binding characteristics of calsequestrin (CSQ) have been estimated from studies of cardiac myocytes. Its Kd has been previously shown to be 0.630 mM (54), with a B_{max} of 2.7 ± 0.2 mM SR (20). Values for intra-SR [Ca^{2+}] were converted from units of μmol/l cytosol to μM SR by assuming the SR volume is 3.5% of the total cell volume and that 65% of the cell volume is cytosol (55). The final conversion factor was 18.1 L cytosol/L SR. This information allowed quantification of the $[Ca^{2+}]_{SR}$.

SUPPLEMENTARY MATERIAL

To view all of the supplemental files associated with this article, visit www.biophysj.org.

We gratefully acknowledge financial support from the British Heart Foundation and the Engineering and Physical Sciences Research Council.

REFERENCES

1. Cheng, H., W. J. Lederer, and M. B. Cannell. 1993. Ca^{2+} sparks: elementary events underlying excitation-contraction coupling in heart muscle. *Science*. 262:740–744.
2. Kort, A. A., M. C. Capogrossi, and E. G. Lakatta. 1985. Frequency, amplitude, and propagation velocity of spontaneous Ca^{2+}-dependent contractile waves in intact adult rat cardiac muscle and isolated myocytes. *Circ. Res.* 57:844–855.
3. Wier, W. G., M. B. Cannell, J. R. Berlin, E. Marban, and W. J. Lederer. 1987. Cellular and subcellular heterogeneity of $[Ca^{2+}]_i$ in single heart cells revealed by Fura-2. *Science*. 235:325–328.
4. Takamatsu, T., and W. G. Wier. 1990. Ca^{2+} waves in mammalian heart: quantification of origin, magnitude, waveform, and velocity. *FASEB J.* 4:1519–1525.
5. Cheng, H., M. R. Lederer, W. J. Lederer, and M. B. Cannell. 1996. Ca^{2+} sparks and $[Ca^{2+}]_i$ waves in cardiac myocytes. *Am. J. Physiol.* 270:C148–C159.
6. Stern, M. D., M. C. Capogrossi, and E. G. Lakatta. 1988. Spontaneous Ca^{2+} release from the sarcoplasmic reticulum in myocardial cells: mechanisms and consequences. *Cell Calcium.* 9:247–256.
7. Diaz, M. E., A. W. Trafford, S. C. O'Neill, and D. A. Eisner. 1997. Measurement of sarcoplasmic reticulum Ca^{2+} content and sarcolemmal Ca^{2+} fluxes in isolated rat ventricular myocytes during spontaneous Ca^{2+} release. *J. Physiol.* 501:3–16.

8. Lederer, W. J., and R. W. Tsien. 1976. Transient inward current underlying arrhythmogenic effects of cardiotonic steroids in Purkinje fibres. *J. Physiol.* 263:73–100.
9. Lukyanenko, V., S. Subramanian, I. Györke, T. F. Wiesner, and S. Györke. 1999. The role of luminal Ca^{2+} in the generation of Ca^{2+} waves in rat ventricular myocytes. *J. Physiol.* 518:173–186.
10. Lukyanenko, V., and S. Györke. 1999. Ca^{2+} sparks and Ca^{2+} waves in saponin-permeabilized rat ventricular myocytes. *J. Physiol.* 521: 575–585.
11. Loughrey, C. M., K. E. MacEachern, P. Neary, and G. L. Smith. 2002. The relationship between intracellular [Ca^{2+}] and Ca^{2+} wave characteristics in permeabilised cardiomyocytes from the rabbit. *J. Physiol.* 543:859–870.
12. Kaneko, T., H. Tanaka, M. Oyamada, S. Kawata, and T. Takamatsu. 2000. Three distinct types of Ca^{2+} waves in Langendorff-perfused rat heart revealed by real-time confocal microscopy. *Circ. Res.* 86:1093–1099.
13. Izu, L. T., W. G. Wier, and C. W. Balke. 2001. Evolution of cardiac calcium waves from stochastic calcium sparks. *Biophys. J.* 80: 103–120.
14. Keizer, J., and G. D. Smith. 1998. Spark-to-wave transition: saltatory transmission of calcium waves in cardiac myocytes. *Biophys. Chem.* 72:87–100.
15. Subramanian, S., S. Viatchenko-Karpinski, V. Lukyanenko, S. Györke, and T. F. Wiesner. 2001. Underlying mechanisms of symmetric calcium wave propagation in rat ventricular myocytes. *Biophys. J.* 80:1–11.
16. Neary, P., A. M. Duncan, S. M. Cobbe, and G. L. Smith. 2002. Assessment of sarcoplasmic reticulum Ca^{2+} flux pathways in cardiomyocytes from rabbits with infarct-induced left-ventricular dysfunction. *Pflugers Arch.* 444:360–371.
17. Loughrey, C. M., K. E. MacEachern, J. Cooper, and G. L. Smith. 2003. Measurement of the dissociation constant of Fluo-3 for Ca^{2+} in isolated rabbit cardiomyocytes using Ca^{2+} wave characteristics. *Cell Calcium.* 34:1–9.
18. Wu, X., and D. M. Bers. 2006. Sarcoplasmic reticulum and nuclear envelope are one highly interconnected Ca^{2+} store throughout cardiac myocyte. *Circ. Res.* 99:283–291.
19. Swietach, P., K. W. Spitzer, and R. D. Vaughan-Jones. 2007. Effective calcium mobility inside the sarcoplasmic reticulum is low. 2007 Biophysical Society Meeting Abstracts. *Biophys. J.* 94a. (Abstr.). 1220-Pos.
20. Shannon, T. R., K. S. Ginsburg, and D. M. Bers. 2000. Reverse mode of the sarcoplasmic reticulum calcium pump and load-dependent cytosolic calcium decline in voltage-clamped cardiac ventricular myocytes. *Biophys. J.* 78:322–333.
21. Hove-Madsen, L., and D. M. Bers. 1993. Passive Ca^{2+} buffering and SR Ca^{2+} uptake in permeabilized rabbit ventricular myocytes. *Am. J. Physiol.* 264:C677–C686.
22. Shannon, T. R., K. S. Ginsburg, and D. M. Bers. 2002. Quantitative assessment of the SR Ca^{2+} leak-load relationship. *Circ. Res.* 91: 594–600.
23. Maier, L. S., and D. M. Bers. 2002. Calcium, calmodulin, and calcium-calmodulin kinase II: heartbeat to heartbeat and beyond. *J. Mol. Cell. Cardiol.* 34:919–939.
24. Kubalova, Z., I. Györke, R. Terentyeva, S. Viatchenko-Karpinski, D. Terentyev, S. C. Williams, and S. Györke. 2004. Modulation of cytosolic and intra-sarcoplasmic reticulum Ca^{2+} waves by calsequestrin in rat cardiac myocytes. *J. Physiol.* 561:515–524.
25. Kubalova, Z., D. Terentyev, S. Viatchenko-Karpinski, Y. Nishijima, I. Györke, R. Terentyeva, D. N. da Cunha, A. Sridhar, D. S. Feldman, R. L. Hamlin, C. A. Carnes, and S. Györke. 2005. Abnormal intrastore calcium signaling in chronic heart failure. *Proc. Natl. Acad. Sci. USA.* 102:14104–14109.
26. Currie, S., C. M. Loughrey, M. A. Craig, and G. L. Smith. 2004. Calcium/calmodulin-dependent protein kinase IIdelta associates with the ryanodine receptor complex and regulates channel function in rabbit heart. *Biochem. J.* 377:357–366.
27. Duchen, M. R., A. Leyssens, and M. Crompton. 1998. Transient mitochondrial depolarizations reflect focal sarcoplasmic reticular calcium release in single rat cardiomyocytes. *J. Cell Biol.* 142:975–988.
28. Maack, C., S. Cortassa, M. A. Aon, A. N. Ganesan, T. Liu, and B. O'Rourke. 2006. Elevated cytosolic Na^{+} decreases mitochondrial Ca^{2+} uptake during excitation-contraction coupling and impairs energetic adaptation in cardiac myocytes. *Circ. Res.* 99:172–182.
29. Bassani, R. A., and D. M. Bers. 1995. Rate of diastolic Ca^{2+} release from the sarcoplasmic reticulum of intact rabbit and rat ventricular myocytes. *Biophys. J.* 68:2015–2022.
30. Smith, G. D., J. E. Keizer, M. D. Stern, W. J. Lederer, and H. Cheng. 1998. A simple numerical model of calcium spark formation and detection in cardiac myocytes. *Biophys. J.* 75:15–32.
31. Sipido, K. R., and W. G. Wier. 1991. Flux of Ca^{2+} across the sarcoplasmic reticulum of guinea-pig cardiac cells during excitation-contraction coupling. *J. Physiol.* 435:605–630.
32. Berlin, J. R., J. W. Bassani, and D. M. Bers. 1994. Intrinsic cytosolic Ca^{2+} buffering properties of single rat cardiac myocytes. *Biophys. J.* 67:1775–1787.
33. Shannon, T. R., K. S. Ginsburg, and D. M. Bers. 2000. Potentiation of fractional sarcoplasmic reticulum Ca^{2+} release by total and free intra-sarcoplasmic reticulum Ca^{2+} concentration. *Biophys. J.* 78: 334–343.
34. Greenstein, J. L., and R. L. Winslow. 2002. An integrative model of the cardiac ventricular myocyte incorporating local control of Ca^{2+} release. *Biophys. J.* 83:2918–2945.
35. Luo, C. H., and Y. Rudy. 1994. A dynamic model of the cardiac ventricular action potential. II. Afterdepolarizations, triggered activity, and potentiation. *Circ. Res.* 74:1097–1113.
36. Snyder, S. M., B. M. Palmer, and R. L. Moore. 2000. A mathematical model of cardiocyte Ca^{2+} dynamics with a novel representation of sarcoplasmic reticular Ca^{2+} control. *Biophys. J.* 79:94–115.
37. Trafford, A. W., P. Lipp, S. C. O'Neill, E. Niggli, and D. A. Eisner. 1995. Propagating Ca^{2+} waves initiated by local caffeine application in rat ventricular myocytes. *J. Physiol.* 489:319–326.
38. Stern, M. D. 1992. Theory of excitation-contraction coupling in cardiac muscle. *Biophys. J.* 63:497–517.
39. Györke, I., and S. Györke. 1998. Regulation of the cardiac ryanodine receptor channel by luminal Ca^{2+} involves luminal Ca^{2+} sensing sites. *Biophys. J.* 75:2801–2810.
40. Györke, I., N. Hester, L. R. Jones, and S. Györke. 2004. The role of calsequestrin, triadin, and junctin in conferring cardiac ryanodine receptor responsiveness to luminal calcium. *Biophys. J.* 86:2121–2128.
41. O'Neill, S. C., L. Miller, R. Hinch, and D. A. Eisner. 2004. Interplay between SERCA and sarcolemmal Ca^{2+} efflux pathways controls spontaneous release of Ca^{2+} from the sarcoplasmic reticulum in rat ventricular myocytes. *J. Physiol.* 559:121–128.
42. Keller, M., J. P. Kao, M. Egger, and E. Niggli. 2007. Ca^{2+} waves driven by ''sensitization'' wave-fronts. *Cardiovasc. Res.* 74:39–45.
43. Mattiazzi, A., L. Hove-Madsen, and D. M. Bers. 1994. Protein kinase inhibitors reduce SR Ca^{2+} transport in permeabilized cardiac myocytes. *Am. J. Physiol.* 267:H812–H820.
44. DeSantiago, J., L. S. Maier, and D. M. Bers. 2002. Frequency-dependent acceleration of relaxation in the heart depends on CaMKII, but not phospholamban. *J. Mol. Cell. Cardiol.* 34:975–984.
45. Valverde, C. A., C. Mundiña-Weilenmann, M. Said, P. Ferrero, L. Vittone, M. Salas, J. Palomeque, M. V. Petroff, and A. Mattiazzi. 2005. Frequency-dependent acceleration of relaxation in mammalian heart: a property not relying on phospholamban and SERCA2a phosphorylation. *J. Physiol.* 562:801–813.
46. Witcher, D. R., R. J. Kovacs, H. Schulman, D. C. Cefali, and L. R. Jones. 1991. Unique phosphorylation site on the cardiac ryanodine receptor regulates calcium channel activity. *J. Biol. Chem.* 266:11144–11152.

47. Lokuta, A. J., T. B. Rogers, W. J. Lederer, and H. H. Valdivia. 1995. Modulation of cardiac ryanodine receptors of swine and rabbit by a phosphorylation-dephosphorylation mechanism. *J. Physiol.* 487: 609–622.

48. Maier, L. S., T. Zhang, L. Chen, J. DeSantiago, J. H. Brown, and D. M. Bers. 2003. Transgenic CaMKIIdeltaC overexpression uniquely alters cardiac myocyte Ca^{2+} handling: reduced SR Ca^{2+} load and activated SR Ca^{2+} release. *Circ. Res.* 92:904–911.

49. Zhang, T., L. S. Maier, N. D. Dalton, S. Miyamoto, J. Ross, D. M. Bers, and J. H. Brown. 2003. The deltaC isoform of CaMKII is activated in cardiac hypertrophy and induces dilated cardiomyopathy and heart failure. *Circ. Res.* 92:912–919.

50. Ai, X., J. W. Curran, T. R. Shannon, D. M. Bers, and S. M. Pogwizd. 2005. Ca^{2+}/calmodulin-dependent protein kinase modulates cardiac ryanodine receptor phosphorylation and sarcoplasmic reticulum Ca^{2+} leak in heart failure. *Circ. Res.* 97:1314–1322.

51. Neumann, J., T. Eschenhagen, L. R. Jones, B. Linck, W. Schmitz, H. Scholz, and N. Zimmermann. 1997. Increased expression of cardiac phosphatases in patients with end-stage heart failure. *J. Mol. Cell. Cardiol.* 29:265–272.

52. Currie, S., and G. L. Smith. 1999. Calcium/calmodulin-dependent protein kinase II activity is increased in sarcoplasmic reticulum from coronary artery ligated rabbit hearts. *FEBS Lett.* 459:244–248.

53. Shannon, T. R., K. S. Ginsburg, and D. M. Bers. 1998. Reverse mode of the sarcoplasmic reticulum Ca^{2+} pump limits sarcoplasmic reticulum Ca^{2+} uptake in permeabilised and voltage clamped myocytes. *Ann. N. Y. Acad. Sci.* 853:350–352.

54. Shannon, T. R., and D. M. Bers. 1997. Assessment of intra-SR free [Ca^{2+}] and buffering in rat heart. *Biophys. J.* 73:1524–1531.

55. Page, E., L. P. McCallister, and B. Power. 1971. Sterological measurements of cardiac ultrastructures implicated in excitation-contraction coupling. *Proc. Natl. Acad. Sci. USA.* 68:1465–1466.